On long-wave propagation over a fluid-mud seabed

PHILIP L.-F. LIU AND I-CHI CHAN

School of Civil and Environmental Engineering, Cornell University, Ithaca, NY 14853, USA

Using the Boussinesq approximation, a set of depth-integrated wave equations for long-wave propagation over a mud bed is derived. The wave motions above the mud bed are assumed to be irrotational and the mud bed is modelled as a highly viscous fluid. The pressure and velocity are required to be continuous across the water–mud interface. The resulting governing equations are differential–integral equations in terms of the depth-integrated horizontal velocity and the free-surface displacement. The effects of the mud bed appear in the continuity equation in the form of a time integral of weighted divergence of the depth-averaged velocity. Damping rates for periodic waves and solitary waves are calculated. For the solitary wave case, the velocity profiles in the water column and the mud bed at different phases are discussed. The effects of the viscous boundary layer above the mud–water interface are also examined.

1. Introduction

Most studies of wave–seabed interactions have focused on wave propagation over non-cohesive sediments (i.e. a sandy bed) (e.g. Liu 1973). Wave attenuation due to percolation in a sandy bed tends to be relatively minor in comparison with other dissipative mechanisms, such as bottom roughness and wave breaking. On the other hand, it is well known that damping of ocean waves can be considerable, if the seabed consists of cohesive sediments. Gade (1958) reported that there is a location in the Gulf of Mexico, called the Mud Hole, where the attenuation of ocean waves due to the mud bed is so great that fishing boats use it as an emergency harbour during storms. Similar mud beds have been reported in many coasts, rivers and estuaries around the world (Healy, Wang & Healy 2002). The dynamic behaviour of cohesive sediments is complex. Many constitutive models have been suggested, including the viscous fluid (Dalrymple & Liu 1978), visco-elastic (MacPherson 1980) and poro-elastic models (Yamamoto *et al.* 1978). Wen & Liu (1998) classified the applicability of these models based on soil properties. It is clear that because of the great complexity and variety of mud rheology, no single model can describe the entire spectrum of the mud bed responses. On the other hand, each model has its own range of validity and it is worthwhile pursuing a deeper understanding of each one. In this paper, we shall focus on the mud layer that can be modelled as a highly viscous fluid.

Within the framework of linear periodic wave theory, many researchers have investigated the effects of a viscous fluid-mud bed on wave propagation (e.g. Gade 1958; Dalrymple & Liu 1978; Ng 2000). However, seabed effects become more significant as water waves propagate into shallow water where the wave system is better described by Boussinesq-type wave equations (e.g. Peregrine 1972). Therefore, it

is the objective of this paper to derive a set of Boussinesq-type equations for weakly nonlinear and weakly dispersive waves with the effects of viscous fluid-mud bed considered. The perturbation approach presented in Liu & Orfila (2004) is adopted in the present study. In the fluid–mud system, we consider the mud viscosity to be several orders of magnitude larger than that of water. Furthermore, we assume that the thickness of the mud bed is very thin so that the pressure is vertically uniform within the mud bed. The leading-order water–mud interfacial conditions are the continuity of the vertical velocity component and the free shear stress condition. A set of depth-integrated continuity and momentum equations is derived. The leading-order effects of a mud bed on the transient long wave appear in the continuity equation in the form of a time integral of weighted divergence of the depth-averaged acceleration. These equations can be used as a base for a large-scale wave propagation model with the effects of mud bed considered. The results for damping rates of periodic waves and solitary waves are also presented. As expected, the wave attenuation due to the mud bed is much more significant than the damping caused by the viscous effects of water. In the case of a solitary wave, the details of the horizontal velocity profiles in the entire water column and the mud bed are discussed.

2. Formulation

Consider a wavetrain with the surface displacement $\zeta'(x', y', t')$ propagating in a constant water depth, h'. The viscous fluid-mud bed has a thickness, d'. The wave motions are characterized by the typical wave amplitude, a'_0, the horizontal length scale, l'_o, which is related to the magnitude of wavelength, and the time scale, $l'_o/\sqrt{gh'}$. The following dimensionless variables are introduced:

$$
\begin{aligned}
(x, y) = (x', y')/l'_o, \quad z = z'/h', \quad t = t'\sqrt{gh'}/l'_o, \\
\zeta = \zeta'/a'_0, \quad p = p'/\rho_w g a'_0, \\
(u, v) = (u', v')/\epsilon\sqrt{gh'}, \quad w = w'\mu/\epsilon\sqrt{gh'},
\end{aligned}
\tag{2.1}
$$

in which p' denotes the pressure, (u', v') the horizontal fluid velocity components in the (x', y')-directions, w' the vertical fluid velocity component in the z'-direction, ρ_w the fluid density, and g the gravitational acceleration. Two dimensionless parameters

$$
\epsilon = a'_0/h', \quad \mu = h'/l'_o,
\tag{2.2}
$$

have been introduced to measure the relative importance of the nonlinearity and the frequency dispersion.

We assume that the viscosity of water is much smaller than that of the viscous fluid mud so that the viscosity of the water can be ignored. However, the viscous effects of water will be discussed in Appendix A. In terms of velocity potential, Φ, the continuity equation for wave motions can be expressed as

$$
\mu^2 \nabla^2 \Phi + \frac{\partial^2 \Phi}{\partial z^2} = 0, \quad -1 < z < \epsilon\zeta.
\tag{2.3}
$$

The dynamic and kinematic free-surface boundary conditions require

$$
\mu^2 \left(\frac{\partial \Phi}{\partial t} + \zeta \right) + \frac{1}{2}\epsilon \left[\mu^2 |\nabla\Phi|^2 + \left(\frac{\partial \Phi}{\partial z} \right)^2 \right] = 0, \quad z = \epsilon\zeta,
\tag{2.4}
$$

$$
\mu^2 \left[\frac{\partial \zeta}{\partial t} + \epsilon \nabla\Phi \cdot \nabla\zeta \right] = \frac{\partial \Phi}{\partial z}, \quad z = \epsilon\zeta,
\tag{2.5}
$$

in which the atmospheric pressure has been assumed to be zero.

On the other hand, viscous effects dominate in the mud bed. We further assume that the mud layer is very thin and is of the same order of magnitude as the viscous mud boundary layer. Hence, in the mud bed, the dimensionless mud flow velocity components are re-scaled as

$$(u_m, v_m) = (u'_m, v'_m)/\epsilon \sqrt{gh'}, \quad w_m = w'_m/\alpha\epsilon \sqrt{gh'}, \tag{2.6}$$

in which

$$\alpha^2 = \frac{\nu_m}{l'_o \sqrt{gh'}}, \tag{2.7}$$

with ν_m being the kinematic viscosity of the viscous mud, can be viewed as the inverse of a Reynolds number. The order of magnitude of the boundary-layer thickness δ'_m can be expressed as $O(\alpha l'_o)$. Furthermore the displacement of the water–mud interface is much smaller than that of the free surface (see Appendix B) and can be considered as a horizontal surface, $z = -1$, for the present study. Thus, the model equations for the mud flows can be expressed as

$$\nabla \cdot \boldsymbol{u}_m + \frac{\partial w_m}{\partial \eta} = 0, \quad -(\mu/\alpha)d \leqslant \eta \leqslant 0, \tag{2.8}$$

$$\frac{\partial \boldsymbol{u}_m}{\partial t} = -\gamma \nabla p + \frac{\partial^2 \boldsymbol{u}_m}{\partial \eta^2}, \quad -(\mu/\alpha)d \leqslant \eta \leqslant 0, \tag{2.9}$$

in which

$$\eta = \frac{z+1}{\alpha/\mu} \tag{2.10}$$

is the stretched vertical coordinate and $\gamma = \rho_w/\rho_m$ is the density ratio with ρ_m being the density of viscous mud.

Along the water-mud interface, the pressure is continuous. Furthermore, the continuity of the vertical velocity is required, i.e.

$$\frac{\partial \Phi}{\partial z} = \alpha\mu w_m, \quad \eta = 0. \tag{2.11}$$

Since we have assumed that the water viscosity is negligible, the tangential stress components vanish along the water-mud interface. Thus,

$$\frac{\partial \boldsymbol{u}_m}{\partial \eta} = 0, \quad \eta = 0. \tag{2.12}$$

We remark here that if the effect of water viscosity, ν_w, is not entirely ignored, the shear stress above the water-mud interface is of $O(\sqrt{\nu_w})$, which is much smaller than that of the induced flow in the mud bed, which is $O(\sqrt{\nu_m})$. More discussion on the effects of water viscosity can be found in Appendix A. Along the bottom of the mud bed, $z = -(1+d)$ or $\eta = -(\mu/\alpha)d = -\bar{d}$, the no-slip condition is imposed, i.e.

$$\boldsymbol{u}_m = 0, \quad w_m = 0, \quad \eta = -\bar{d}. \tag{2.13}$$

We reiterate that the approach for the mud flow analysis requires $O(d') \sim O(\delta'_m)$ with δ'_m being the boundary-layer thickness of the mud bed. This also implies that $O(d) \sim O(\alpha/\mu)$ or $O(\bar{d}) \sim O(1)$.

2.1. *Boundary-layer solution inside the mud bed*

In this section, we focus on the flow inside the mud bed. Denoting the horizontal velocity at the water-mud interface as

$$\boldsymbol{u}_b(\boldsymbol{x}, t) = \nabla \Phi(\boldsymbol{x}, z = -1, t), \tag{2.14}$$

the horizontal gradient of the dynamic pressure inside the mud bed can be approximated as

$$\frac{\partial \boldsymbol{u}_b}{\partial t} = -\nabla p. \tag{2.15}$$

Substituting the above equation into (2.9), we obtain

$$\frac{\partial \boldsymbol{u}_m}{\partial t} = \gamma \frac{\partial \boldsymbol{u}_b}{\partial t} + \frac{\partial^2 \boldsymbol{u}_m}{\partial \eta^2}, \quad -\overline{d} \leqslant \eta \leqslant 0. \tag{2.16}$$

Introducing a new variable

$$\boldsymbol{v}_m = \boldsymbol{u}_m - \gamma \boldsymbol{u}_b, \tag{2.17}$$

the boundary-value problem for the boundary-layer mud flow can be expressed in terms of $\boldsymbol{v}_m$ as

$$\frac{\partial \boldsymbol{v}_m}{\partial t} = \frac{\partial^2 \boldsymbol{v}_m}{\partial \eta^2}, \quad -\overline{d} \leqslant \eta \leqslant 0, \tag{2.18}$$

with the following boundary conditions:

$$\frac{\partial \boldsymbol{v}_m}{\partial \eta} = 0, \quad \eta = 0, \tag{2.19}$$

and

$$\boldsymbol{v}_m = -\gamma \boldsymbol{u}_b, \quad \eta = -\overline{d}. \tag{2.20}$$

The analytical solution for the two-point boundary-value problem can be obtained straightforwardly as

$$\boldsymbol{v}_m(\boldsymbol{x}, \eta, t) = -\gamma \int_0^t \frac{\partial \boldsymbol{u}_b}{\partial \tau} \mathrm{erfc} \left[\frac{\eta + \overline{d}}{\sqrt{4(t-\tau)}} \right] \mathrm{d}\tau$$
$$- \gamma \sum_{n=1}^{\infty} (-1)^n \int_0^t \frac{\partial \boldsymbol{u}_b}{\partial \tau} \left[-\mathrm{erfc} \left(\frac{-\eta + (2n-1)\overline{d}}{\sqrt{4(t-\tau)}} \right) + \mathrm{erfc} \left(\frac{\eta + (2n+1)\overline{d}}{\sqrt{4(t-\tau)}} \right) \right] \mathrm{d}\tau. \tag{2.21}$$

From the continuity equation, (2.8), the vertical velocity component can be calculated by integration,

$$w_m(\boldsymbol{x}, \eta, t) = - \int_{-\overline{d}}^{\eta} \nabla \cdot (\boldsymbol{v}_m + \gamma \boldsymbol{u}_b) \, \mathrm{d}\eta'. \tag{2.22}$$

On the mud–water interface, $\eta = 0$, the vertical velocity component becomes

$$w_m(\mathbf{x}, 0, t) = -\gamma \left\{ \overline{d} \nabla \cdot u_b - \int_0^t \frac{\partial \nabla \cdot \boldsymbol{u}_b}{\partial \tau} I(t-\tau) \, \mathrm{d}\tau \right\}, \tag{2.23}$$

where

$$I(t-\tau) = \sqrt{\frac{4(t-\tau)}{\pi}} \left\{ 1 - \exp \left[\frac{-\overline{d}^2}{4(t-\tau)} \right] \right\} + \overline{d} \, \mathrm{erfc} \left(\frac{\overline{d}}{\sqrt{4(t-\tau)}} \right)$$
$$- \sum_{n=1}^{\infty} (-1)^n \left\{ \sqrt{\frac{4(t-\tau)}{\pi}} \left[-3\exp \left(-\frac{(2n\overline{d})^2}{4(t-\tau)} \right) + \sum_{m=-1}^{1} \exp \left(-\frac{((2n+m)\overline{d})^2}{4(t-\tau)} \right) \right] \right.$$
$$+ \overline{d} \left[2n\,\mathrm{erfc} \left(\frac{2n\overline{d}}{\sqrt{4(t-\tau)}} \right) + \sum_{m=-1}^{1} (-1)^m (2n-m)\mathrm{erfc} \left(\frac{(2n-m)\overline{d}}{\sqrt{4(t-\tau)}} \right) \right] \right\}. \tag{2.24}$$
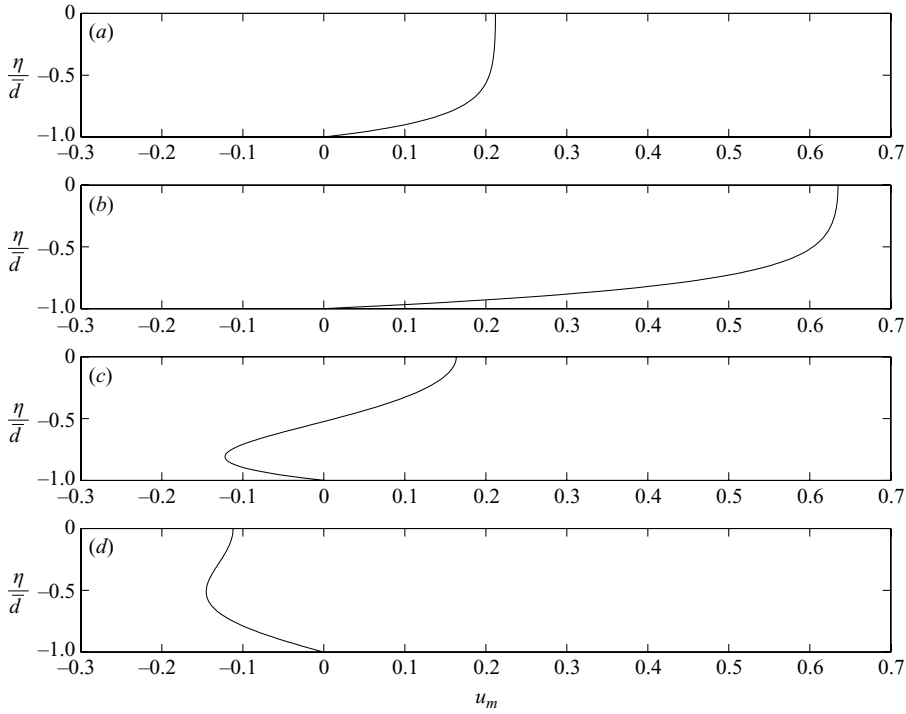
FIGURE 1. Horizontal velocity inside the mud bed at different phases under a solitary wave. (a) $u_b = 0.25$ during the acceleration phase; (b) $u_b = 0.75$ during the acceleration phase; (c) $u_b = 0.25$ during the deceleration phase; (d) $u_b = 0.01$ during the deceleration phase. ($\gamma = 0.85, \epsilon = \mu^2 = 0.1, \alpha = 0.01, \bar{d} = 5, x_0 = -50$.)

The shear stress at the bottom of the mud bed ($\eta = -\bar{d}$) is defined as

$$\tau_{mb} = \frac{\partial \boldsymbol{u}_m}{\partial \eta}, \quad \eta = -\bar{d}, \tag{2.25}$$

and can be calculated by using (2.17) and (2.21). Thus,

$$\tau_{mb} = \frac{\gamma}{\sqrt{\pi}} \int_0^t \frac{\partial \boldsymbol{u}_b}{\partial \tau} \frac{1}{\sqrt{t-\tau}} \left[1 + 2 \sum_{n=1}^{\infty} (-1)^n \exp\left(\frac{(n\bar{d})^2}{t-\tau}\right)\right] d\tau. \tag{2.26}$$

As an example, we calculate the horizontal velocity component within the mud layer under a solitary wave loading. In other words, the horizontal velocity above the water-mud interface, u_b, (2.14), is prescribed by the solitary wave solution as

$$u_b(x, t) = \text{sech}^2 \left[\frac{1}{\mu} \sqrt{\frac{3\epsilon}{4}} (x - x_o - Ct)\right], \tag{2.27}$$

where x_o is the initial position of the wave crest and $C = \sqrt{1 + \epsilon}$ is the dimensionless celerity. In figure 1, profiles of the horizontal velocity in the mud bed are shown at four different phases and the following parameters have been used: $\gamma = 0.85, \epsilon = \mu^2 = 0.1, \alpha = 0.01, \bar{d} = 5, x_0 = -50$. Panels (a) and (b) represent the phases when the mud–water interface velocity accelerates toward its maximum velocity under the wave crest. The velocity is in the same direction as the wave propagation in the entire
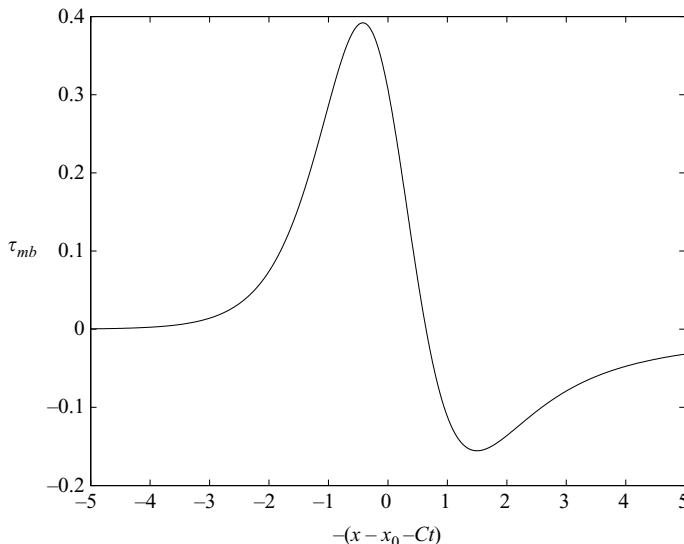
FIGURE 2. Time history of the bottom shear stress in the mud bed, τ_{mb}, under a solitary wave. Positive $(x - x_0 - Ct)$ represents the accelerating phase while the negative portion is the decelerating phase. Parameters are same as in figure 1.

mud bed. From the momentum equation in the horizontal direction, the horizontal pressure gradient is always balanced by the bottom shear stress in the mud bed, τ_{mb}. Once the wave crest passes, the mud–water interface velocity starts to decelerate and the horizontal pressure gradient reverses direction. Consequently, the bottom shear stress in the mud bed must change sign too. Therefore, near the bottom of the mud bed the velocity also reverses direction, while the velocity near the mud–water interface is still in the same direction as wave propagation (see panel *c*). As the mud–water layer slows down further, the horizontal velocity in the entire mud layer moves in the opposite direction to the wave propagation (see panel *d*). The above discussion can be better understood from figure 2, which shows the time history of the bottom shear stress in the mud bed, τ_{mb}. The features shown in these two figures are very similar to those observed in the bottom boundary-layer flow under a solitary wave without a mud bed (Liu, Park & Cowen 2007). More discussion on this topic is given in Appendix A.

3. Boussinesq-type equations

In this section, we present simplified governing equations for the irrotational flow by adopting the Boussinesq approximation, i.e. $O(\epsilon) \sim O(\mu^2)$. We further assume that $O(\alpha) \sim O(\mu^4)$. Following Liu & Orfila's (2004) approach, we expand the potential function as a power series in the vertical coordinate,

$$\Phi(\boldsymbol{x}, z, t) = \sum_{n=0}^{\infty} (z + 1)^n \phi_n(\boldsymbol{x}, t). \tag{3.1}$$

Substituting the expansion into the Laplace equation, (2.3), and the water–mud interfacial condition, (2.11), we obtain the following recursive relation:

$$\phi_{n+2} = \frac{-\mu^2 \nabla^2 \phi_n}{(n+1)(n+2)}, \quad n = 0, 1, 2, \ldots, \tag{3.2}$$

with

$$\phi_1 = \alpha \mu w_m(\mathbf{x}, 0, t), \tag{3.3}$$

in which w_m is given in (2.23).

Using the recursive relation in the expansion, we obtain the potential function truncated up to $O(\mu^5)$:

$$\Phi = \phi_0 + (z+1)\phi_1 - \frac{\mu^2}{2}(z+1)^2\nabla^2\phi_0 + \frac{\mu^4}{24}(z+1)^4\nabla^2\nabla^2\phi_0 + O(\mu^6). \tag{3.4}$$

Defining the horizontal velocity at the water–mud interface and the total water depth as

$$\mathbf{u}_b = \nabla\phi_0, \quad H = 1 + \epsilon\zeta, \tag{3.5}$$

the kinematic free-surface boundary condition, (2.5), becomes

$$\frac{1}{\epsilon}\frac{\partial H}{\partial t} + \nabla\cdot\left[\left(H + \gamma\frac{\alpha}{\mu}\overline{d}\right)\mathbf{u}_b\right] - \frac{\mu^2}{6}\nabla^2\nabla\cdot\mathbf{u}_b - \gamma\frac{\alpha}{\mu}\int_0^t \frac{\partial\nabla\cdot\mathbf{u}_b}{\partial\tau}I(t-\tau)\mathrm{d}\tau = O(\mu^4), \tag{3.6}$$

where $I(t-\tau)$ is given in (2.24). We reiterate that the Boussinesq assumption, i.e. $O(\mu^2) \sim O(\epsilon)$, and the assumptions that $O(\alpha) \sim O(\mu^4)$ and $O(\overline{d}) \sim O(1)$ have been employed.

Similarly, the dynamic free-surface boundary condition, (2.4), can be expressed in terms of H and $\mathbf{u}_b$ as

$$\frac{\partial\mathbf{u}_b}{\partial t} + \epsilon\mathbf{u}_b\cdot\nabla\mathbf{u}_b + \frac{1}{\epsilon}\nabla H - \frac{\mu^2}{2}\frac{\partial}{\partial t}(\nabla\nabla\cdot\mathbf{u}_b) = O(\mu^4). \tag{3.7}$$

Equations (3.6) and (3.7) constitute the Boussinesq equations in terms of the water–mud interface velocity, $\mathbf{u}_b$, and the total depth, H, including consideration of the effects of a viscous fluid-mud bed.

Traditionally, Boussinesq equations are expressed in terms of the depth-averaged horizontal velocity. By definition, the depth-averaged velocity is given as

$$\overline{\mathbf{u}} = \frac{1}{H}\int_{-1}^{\epsilon\zeta} \nabla\Phi \, dz = \mathbf{u}_b - \frac{\mu^2}{6}H^2\nabla^2\mathbf{u}_b + O(\mu^4). \tag{3.8}$$

Substituting the above equation into (3.6) and (3.7), we obtain

$$\frac{1}{\epsilon}\frac{\partial H}{\partial t} + \nabla\cdot\left[\left(H + \gamma\frac{\alpha}{\mu}\overline{d}\right)\overline{\mathbf{u}}\right] - \gamma\frac{\alpha}{\mu}\int_0^t \frac{\partial\nabla\cdot\overline{\mathbf{u}}}{\partial\tau}I(t-\tau)\,\mathrm{d}\tau = O(\mu^4), \tag{3.9}$$

$$\frac{\partial\overline{\mathbf{u}}}{\partial t} + \epsilon\overline{\mathbf{u}}\cdot\nabla\overline{\mathbf{u}} + \frac{1}{\epsilon}\nabla H - \frac{\mu^2}{3}\nabla\nabla\cdot\left(\frac{\partial\overline{\mathbf{u}}}{\partial t}\right) = O(\mu^4). \tag{3.10}$$

If the effects of the viscous mud bed are ignored, i.e. $\alpha \to 0$ and $\overline{d} = 0$, (3.9) and (3.10) reduce to the conventional Boussinesq equations. It is clear that the leading-order effects of the mud bed appear in the mass balance in the water column and mud layer.

3.1. *One-dimensional cases*

To illustrate that the viscous damping of simple harmonic waves and solitary waves can be calculated by the present formulation, we consider one-dimensional problems in this section. Thus, the continuity and momentum equations become

$$\frac{\partial\zeta}{\partial t} + \frac{\partial}{\partial x}\left[\left(1 + \epsilon\zeta + \gamma\frac{\alpha}{\mu}\overline{d}\right)\overline{u}\right] - \gamma\frac{\alpha}{\mu}\int_0^t \frac{\partial^2\overline{u}}{\partial x\partial\tau}I(t-\tau)\,\mathrm{d}\tau = 0, \tag{3.11}$$

$$\frac{\partial \overline{u}}{\partial t} + \epsilon \overline{u} \frac{\partial \overline{u}}{\partial x} + \frac{\partial \zeta}{\partial x} - \frac{\mu^2}{3} \frac{\partial^3 \overline{u}}{\partial x^2 \partial t} = 0. \tag{3.12}$$

3.1.1. *Viscous damping of progressive linear long waves*

For linear progressive waves, (3.11) and (3.12) can be further simplified to

$$\frac{\partial \zeta}{\partial t} + \left(1 + \gamma \frac{\alpha}{\mu} \overline{d}\right) \frac{\partial \overline{u}}{\partial x} - \gamma \frac{\alpha}{\mu} \int_0^t \frac{\partial^2 \overline{u}}{\partial x \partial \tau} I(t - \tau) \, d\tau = 0, \tag{3.13}$$

$$\frac{\partial \overline{u}}{\partial t} + \frac{\partial \zeta}{\partial x} = 0. \tag{3.14}$$

Introducing the moving coordinates

$$\sigma = x - t, \quad \xi = \left(\frac{\alpha}{\mu}\right) t, \tag{3.15}$$

into (3.13) and (3.14) and summing the resulting equations, we obtain

$$\frac{\partial \zeta}{\partial \xi} = -\frac{\gamma}{2} \left[\overline{d} \frac{\partial \zeta}{\partial \sigma} + \int_0^t \frac{\partial^2 \zeta}{\partial \sigma^2} I(t - \tau) \, d\tau\right]. \tag{3.16}$$

Note that $\zeta = \overline{u}$ has been used as a leading-order approximation. Because of the viscous damping, the free-surface displacement can be represented as

$$\zeta = a(\xi) e^{i\sigma}. \tag{3.17}$$

Substituting the solution form, (3.17), into (3.16), we obtain

$$\frac{\partial a}{\partial \xi} = -\frac{\gamma}{2} \left[i\overline{d} - \int_0^\infty e^{iq} I(q) \, dq\right] a(\xi). \tag{3.18}$$

Introducing

$$a = a_0 e^{i\beta \xi}, \quad \beta = \beta_r + i\beta_i, \tag{3.19}$$

where β_i denotes the damping rate, into (3.18), we find

$$\beta_r = -\frac{\gamma}{2} \left[\overline{d} - \int_0^\infty \sin q \, I(q) \, dq\right], \tag{3.20}$$

$$\beta_i = -\frac{\gamma}{2} \int_0^\infty \cos q \, I(q) \, dq. \tag{3.21}$$

In figure 3 the damping rate, β_i, is plotted as a function of the dimensionless thickness of mud bed for $\gamma = 0.85$ and 0.9. The solution agrees with that obtained by MacPherson (1980). However, differences between two models appear for large $\overline{d}$ values. This is because of the thin mud layer assumption employed in the present theory. This figure also shows that the heavier mud, which has a stronger inertia, has less impact on wave damping.

3.1.2. *Viscous damping of solitary waves*

A similar analysis can be carried out for calculating the viscous damping of a solitary wave. Following the approach outlined in the previous section, we can combine (3.11) and (3.12) in the moving frame, $\sigma = x - t$, as

$$\frac{\partial \zeta}{\partial \overline{\xi}} + \frac{3}{2} \zeta \frac{\partial \zeta}{\partial \sigma} + \frac{1}{6} \frac{\mu^2}{\epsilon} \frac{\partial^3 \zeta}{\partial \sigma^3} = -\frac{\gamma \alpha}{2\mu \epsilon} \left[\overline{d} \frac{\partial \zeta}{\partial \sigma} + \int_0^t \frac{\partial^2 \zeta}{\partial \sigma^2} I(t - \tau) \, d\tau\right], \tag{3.22}$$
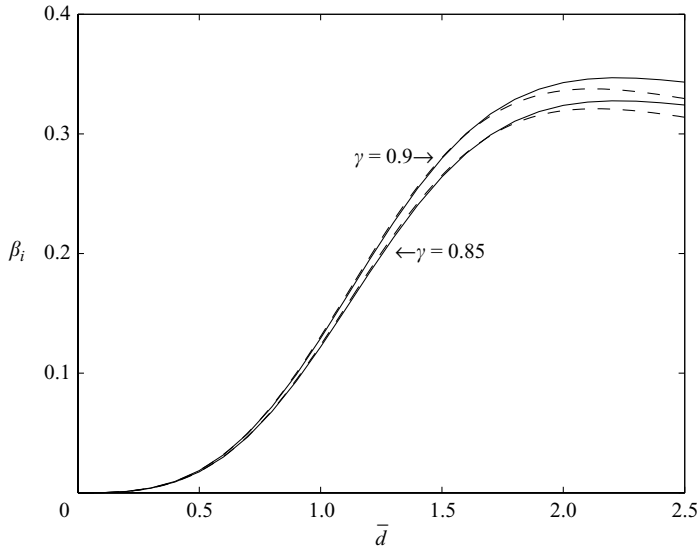
FIGURE 3. Damping rate of small-amplitude periodic waves with different γ. The solid lines represent the present solution and the dashed lines denote the result by MacPherson (1980).

in which the slow time variable is defined as $\bar{\bar{\xi}} = \epsilon t$. Without the damping effect, i.e. $\alpha \to 0$ and $\bar{d} = 0$, the solitary wave solution can be written as

$$\zeta = a(\bar{\bar{\xi}})\text{sech}^2 \left[\frac{\sqrt{3a}}{2} \left(\sigma - \frac{a}{2}\bar{\bar{\xi}} \right) \right]. \tag{3.23}$$

Thus, in considering a viscous mud bed, we introduce the perturbation solution as follows (Liu & Orfila 2004; Mei, Stiassnie & Yue 2005):

$$\zeta = \zeta_0(\rho, \xi) + \delta\zeta_1(\rho, \xi) + \cdots, \tag{3.24}$$

where

$$\rho = \sigma - \frac{1}{2\delta} \int^\xi a(\xi')\,\mathrm{d}\xi', \quad \xi = \delta\bar{\bar{\xi}}, \quad \delta = \frac{\alpha}{\mu\epsilon}. \tag{3.25}$$

Substituting of (3.24) into (3.22) and collecting terms at different orders, we obtain the following equations for the first two orders in δ:

$$L_0\zeta_0 = \frac{\partial}{\partial\rho} \left[-\frac{a}{2} + \frac{3}{4}\zeta_0 + \frac{1}{6}\frac{\mu^2}{\epsilon}\frac{\partial^2}{\partial\rho^2} \right] \zeta_0 = 0, \tag{3.26}$$

$$L_1\zeta_1 = \frac{\partial}{\partial\rho} \left[-\frac{a}{2} + \frac{3}{2}\zeta_0 + \frac{1}{6}\frac{\mu^2}{\epsilon}\frac{\partial^2}{\partial\rho^2} \right] \zeta_1 = -\frac{\gamma}{2} \left[\bar{d}\frac{\partial\zeta_0}{\partial\rho} + \int_0^t \frac{\partial^2\zeta_0}{\partial\rho^2}I(t-\tau)\,\mathrm{d}\tau \right] - \frac{\partial\zeta_0}{\partial\xi}, \tag{3.27}$$

where L_0 and L_1 are adjoint operators of each other (Ott & Sudan 1970), i.e.

$$\int_{-\infty}^{\infty} (\zeta_0 L_1\zeta_1 - \zeta_1 L_0\zeta_0)\,\mathrm{d}\rho = 0. \tag{3.28}$$

Clearly the solution for the leading-order equation is just the solitary wave solution,

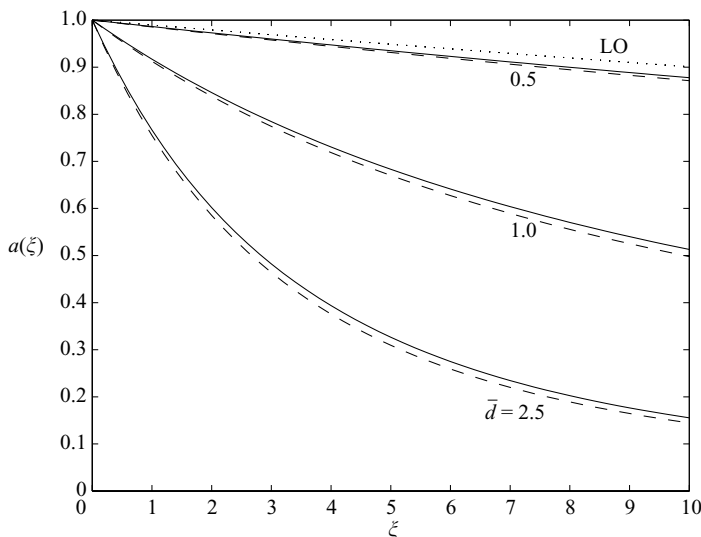$$\zeta_0 = a(\xi)\text{sech}^2 \left[\frac{\sqrt{3a}}{2}\rho \right]. \tag{3.29}$$

FIGURE 4. Wave amplitude, a, as a function of time, ξ. The dotted line denotes the viscous damping caused by the bottom boundary layer including consideration of only water viscosity (Liu & Orfila 2004)(LO). Other curves represent the damping rates induced by the mud bed with different thickness. Solid lines are for $\gamma = 0.85$ and dashed lines $\gamma = 0.9$. To compare LO with the current study, $\nu_m/\nu_w = 10^3$ has been used in the computations.

Equation (3.28) provides a solvability condition for ζ_1

$$\int_{-\infty}^{\infty} \zeta_0 \left\{ \frac{\partial \zeta_0}{\partial \xi} + \frac{\gamma}{2} \left[\bar{d} \frac{\partial \zeta_0}{\partial \rho} + \int_0^t \frac{\partial^2 \zeta_0}{\partial \rho^2} I(t - \tau) \, d\tau \right] \right\} d\rho = 0. \tag{3.30}$$

The items in the integrand of the above integral can be expressed explicitly as

$$-\frac{\partial \zeta_0}{\partial \xi} = -\frac{da}{d\xi} \operatorname{sech}^2 \left(\frac{\sqrt{3a}}{2} \rho \right) \left[1 - \frac{\sqrt{3a}}{2} \rho \tanh \left(\frac{\sqrt{3a}}{2} \rho \right) \right],$$

$$\frac{\partial \zeta_0}{\partial \rho} = -a\sqrt{3a} \operatorname{sech}^2 \left(\frac{\sqrt{3a}}{2} \rho \right) \tanh \left(\frac{\sqrt{3a}}{2} \rho \right),$$

$$\frac{\partial^2 \zeta_0}{\partial \rho^2} = -\frac{3a^2}{2} \operatorname{sech}^4 \left(\frac{\sqrt{3a}}{2} \rho \right) \left[2 - \cosh(\sqrt{3a}\rho) \right].$$

Thus, substituting the above expressions and (3.29) into the solvability condition, (3.30), we find

$$\frac{da}{d\xi} = \frac{\sqrt{3}}{2} \gamma a^{3/2} \int_{-\infty}^{\infty} \int_0^{\infty} \operatorname{sech}^2(R) \operatorname{sech}^4(R + S) \left[2 - \cosh 2(R + S) \right] I \left(\frac{2S}{\sqrt{3a}} \right) dR \, dS. \tag{3.31}$$

The above equation can be integrated numerically to find the time variation of solitary wave amplitudes for a prescribed set of wave data.

Figure 4 displays the numerical results of (3.31) for different mud bed thickness. A forward differencing scheme is used to evaluate the derivative on the left-hand side of (3.31). For the integration on the right-hand side, an adaptive quadrature method with tolerance of 10^{-8} is employed. Clearly, it shows again that the heavier mud has

less impact on the wave damping. To demonstrate the significant damping effect of viscous mud, we compare the present results with Liu & Orfila (2004) in which they consider only the water viscosity in the bottom boundary layer. A viscosity ratio $\nu_m/\nu_w = 10^3$ is used in the computations.

4. Concluding remarks

A set of two-dimensional depth-averaged continuity and momentum equations including consideration of the effects of a viscous fluid-mud bed has been derived, (3.9) and (3.10). The leading-order effects of the mud bed appear in the continuity equation in a form of convolution integral. These equations can also be expressed in terms of the velocity at the water–mud interface, (3.6) and (3.7). The effects of water viscosity are discussed in Appendix A.

The new equations have been employed to obtain the damping rates of periodic waves and solitary waves. While the damping rate for periodic waves agrees with the existing theory, the damping rate for solitary waves is new. The detailed velocity field as well as the damping rate for a solitary wave will be verified by an experimental study similar to those presented in Liu *et al.* (2006, 2007).

Appendix A. Boundary-layer modification above the water–mud interface

The water viscosity has been neglected in the main part of the papers. However, we can include its effect by adding a boundary layer above the water–mud interface. Following Liu & Orfila's (2004) analysis, we introduce the following perturbation expansions for the velocity field inside this interfacial boundary layer:

$$\boldsymbol{u} = \nabla\Phi(x, z, t) + \boldsymbol{u}_0^r(x, z, t) + \alpha_1 \boldsymbol{u}_1^r(x, z, t) + \cdots, \tag{A 1}$$

$$w = \frac{\partial\Phi}{\partial z} + \alpha_1 \mu w_1^r + \cdots, \tag{A 2}$$

in which

$$\alpha_1^2 = \frac{\nu_w}{l_o' \sqrt{gh'}}. \tag{A 3}$$

We note that the thickness of the interfacial boundary layer is $O(\alpha_1)$ and is much smaller than $O(\alpha)$ (i.e. the boundary-layer thickness of the mud bed), therefore inclusion of the interfacial boundary layer will not change the analysis presented in this paper. We introduce the stretched coordinate for the boundary layer

$$\overline{\eta} = \frac{z + 1}{\alpha_1/\mu}. \tag{A 4}$$

The leading-order continuity equation and the horizontal momentum equation for the rotational velocity in the interfacial boundary layer become

$$\nabla \cdot \boldsymbol{u}_0^r + \frac{\partial w_1^r}{\partial \overline{\eta}} = 0, \tag{A 5}$$

$$\frac{\partial \boldsymbol{u}_0^r}{\partial t} + \epsilon \left[\boldsymbol{u}_0^r \cdot \nabla \boldsymbol{u}_0^r + w_1^r \frac{\partial \boldsymbol{u}_0^r}{\partial \overline{\eta}} \right] = \frac{\partial^2 \boldsymbol{u}_0^r}{\partial \overline{\eta}^2}. \tag{A 6}$$

The no-slip conditions on the water–mud interface require that the rotational velocity satisfies the following boundary conditions:

$$\boldsymbol{u}_0^r = -\nabla\Phi + \boldsymbol{u}_m, \quad \frac{\partial\Phi}{\partial z} = -\alpha_1\mu w_1^r + \alpha\mu w_m, \quad \bar{\eta} = 0. \tag{A 7}$$

At the outer edge of the interfacial boundary layer, $\bar{\eta} \to \infty$, both horizontal and vertical rotational velocity components vanish,

$$\boldsymbol{u}_0^r, \ w_1^r \to 0, \quad \bar{\eta} \to \infty. \tag{A 8}$$

We remark here that the horizontal mud flow velocity at the water–mud interface, $\boldsymbol{u}_m$, is related to $\nabla\Phi(\boldsymbol{x}, z = -1, t) = \boldsymbol{u}_b$ and is given in (2.17) and (2.21).

To find the boundary-layer solution for a general transient wave, the boundary-layer equation, (A 6), is linearized:

$$\frac{\partial\boldsymbol{u}_0^r}{\partial t} = \frac{\partial^2\boldsymbol{u}_0^r}{\partial\bar{\eta}^2}. \tag{A 9}$$

The analytical solution can be found as (Liu & Orfila 2004)

$$\boldsymbol{u}_0^r(x, \bar{\eta}, t) = -\frac{\bar{\eta}}{\sqrt{4\pi}} \int_0^t \frac{[\boldsymbol{u}_b - \boldsymbol{u}_m]}{\sqrt{(t-\tau)^3}} \, e^{-\bar{\eta}^2/4(t-\tau)} \, d\tau, \tag{A 10}$$

which is of the same order of magnitude as the irrotational velocity and the mud flow velocity. From the continuity equation, (A 5), the vertical rotational velocity component can be obtained by integration,

$$w_1^r(\mathbf{x}, \bar{\eta}, t) = -\int_{\bar{\eta}}^{\infty} d\eta' \frac{\eta'}{2\sqrt{\pi}} \int_0^t \frac{\nabla^2\Phi(\boldsymbol{x}, z = -1, \tau) - \nabla\cdot\boldsymbol{u}_m}{\sqrt{(t-\tau)^3}} e^{-\eta'^2/4(t-\tau)} \, d\tau. \tag{A 11}$$

At the water–mud interface, the vertical rotational velocity becomes

$$w_1^r(\mathbf{x}, 0, t) = \frac{1}{\sqrt{\pi}} \int_0^t \frac{\nabla^2\Phi(\boldsymbol{x}, z = -1, \tau) - \nabla\cdot\boldsymbol{u}_m}{\sqrt{(t-\tau)^3}} \, d\tau. \tag{A 12}$$

The existence of this rotational vertical velocity component requires a further correction to the irrotational velocity potential in order to satisfy the continuity of vertical velocity along the water–mud interface, (A 7). However, we reiterate here that since the viscosity of water is much smaller than the viscosity of the mud bed, i.e. $\alpha_1 << \alpha$, the vertical velocity of the mud flow is much stronger than the contribution induced by the interfacial boundary layer (see (A 7)). Finally, we note that the shear stress is scaled by the square root of the viscosity. Since $\nu_m >> \nu_w$, to the leading-order the continuity of shear stress at the water–mud interface still yields the same boundary condition as shown in (2.12).

Figure 5 shows profiles of the horizontal velocity component under a solitary wave with the leading-order interfacial boundary layer correction. The continuity of the horizontal velocity component along the water–mud interface is now satisfied. The panels on the left present the velocity profiles in the entire mud bed and a portion of the water column above, while the panels on the right show the details in the vicinity of the water–mud interface. Similarly to figure 1, four different phases are shown. Panels (*a*) and (*b*) represent the phases when the velocity in the water column is accelerating toward its maximum velocity under the wave crest. During the acceleration phase, the velocity in the entire column moves in the same direction as wave propagation. The magnitude of the velocity inside the mud bed is smaller because of the stronger viscous effects. Once the wave crest has passed, the water
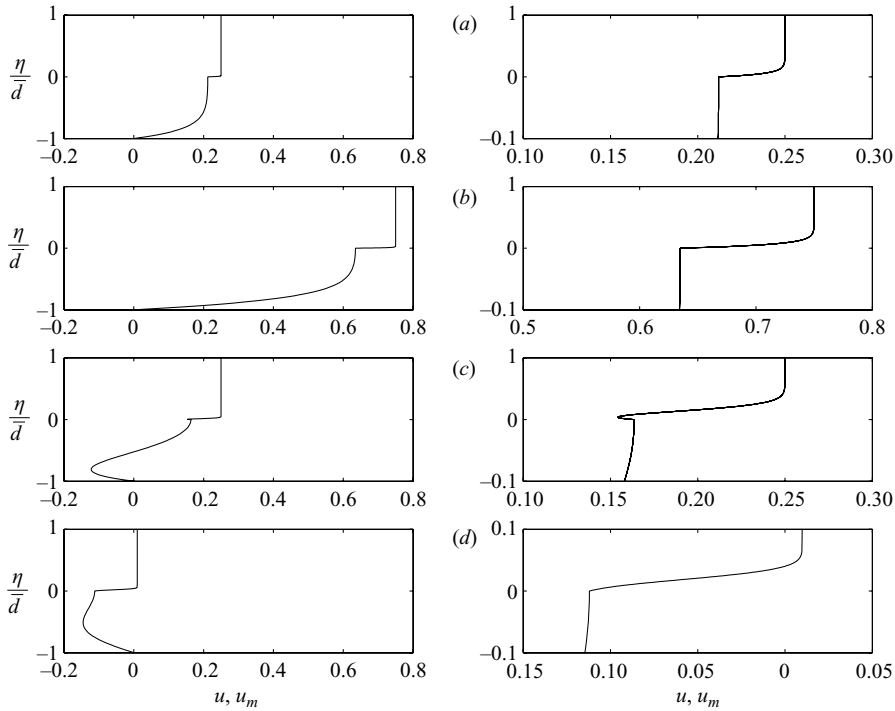
FIGURE 5. Horizontal velocity components at different phases including consideration of the interfacial boundary layer. The left column shows the velocity profiles in the entire mud bed and a portion of the water column above, while the right column presents the velocity profiles in the vicinity of the interface between the water and mud bed. The phase of each case is the same as in figure 1. In (*a*) and (*b*) the wave is accelerating toward the wave crest; (*c*) and (*d*) the deceleration phases. $\nu_m/\nu_w = 10^3$ is used and other parameters are the same as in figure 1.

particles start to decelerate above the water–mud interface, while the horizontal pressure gradient reverses direction. Consequently, near the water–mud interface and the bottom of the mud bed the velocity also reverses direction such that the frictional stresses at the water–mud interface and the bottom of the mud bed respectively can counter-balance the pressure gradient (see panel *c*). As the wave slows down further, the horizontal velocity in the entire mud bed moves in the opposite direction to the wave propagation and pulls the velocity inside the interfacial boundary layer with it (see panel *d*). We note that a small overshoot appears in the interfacial boundary layer, which is expected because of the force balance between the pressure gradient and the shear stress along the water–mud interface.

Appendix B. The order of magnitude of the interfacial displacement

In the present study, the interfacial displacement is neglected, i.e. all interfacial conditions are applied on the still water–mud interface, $\eta = 0$. The justification for this simplification is given here.

For a fully nonlinear problem, the interfacial conditions should be applied at the actual water–mud interface $z = -1 + \epsilon \zeta_m$, with ζ_m being the interfacial displacement. However, in our present analysis we are interested in long waves with a thin mud

bed. Under these conditions, we can show that the interfacial displacement can be neglected.

The continuity equations for the water column above the mud bed and for the mud column can be expressed in terms of depth-averaged velocities as

$$\frac{\partial}{\partial t}(\zeta - \zeta_m) + \nabla \cdot [(1 + \epsilon(\zeta - \zeta_m)\overline{\boldsymbol{u}}] = 0, \tag{B 1}$$

$$\frac{\partial \zeta_m}{\partial t} + \nabla \cdot [(d + \epsilon \zeta_m)\overline{\boldsymbol{u}}_m] = 0. \tag{B 2}$$

Both equations are exact. For long waves we anticipate that $O(\overline{\boldsymbol{u}}) \sim O(\overline{\boldsymbol{u}}_m)$. Let $K = \zeta_m/\zeta$, denoting the ratio between interfacial displacement and the free-surface displacement. Equations (B 1) and (B 2) can be combined to be

$$\left(-\frac{d}{K} + d + 1\right) \nabla \cdot \overline{\boldsymbol{u}}_m = 0. \tag{B 3}$$

Therefore,

$$K = \frac{d}{d+1}. \tag{B 4}$$

Since we have also assumed that the mud bed thickness is comparable with the mud boundary-layer thickness,

$$K = \zeta_m/\zeta \sim d << 1. \tag{B 5}$$

REFERENCES

DALRYMPLE, R. A. & LIU, P. L.-F. 1978 Waves over soft muds: a two layer model. *J. Phys. Oceanogr.* **8**, 1121–1131.

GADE, H. G. 1958 Effects of a non-rigid, impermeable bottom on plane surface waves in shallow water. *J. Mar. Res.* **16**, 61–82.

HEALY, T., WANG, Y., & HEALY, H.-J. 2002 *Muddy Coasts of the World: Processes, Deposits and Function.* Elsevier.

LIU, P. L.-F. 1973 Damping of water waves over porous bed. *J. Hydraul. Div., ASCE* **99**, 2263–2271.

LIU, P. L.-F. & ORFILA, A. 2004 Viscous effects on transient long-wave propagation. *J. Fluid Mech.* **520**, 83–92 (and corrigendum **537**, 2005, 443).

LIU, P. L.-F., SIMARRO, G., VANDEVER, J., & ORFILA, A. 2006 Experimental and numerical investigation of viscous effects on solitary wave propagation in a wave tank. *Coastal Engng.* **53** (2/3), 181–190.

LIU, P. L-F., PARK, Y. S. & COWEN, E. A. 2007 Boundary layer flow and bed shear stress under a solitary wave, *J. Fluid Mech.* **574**, 449–463.

MACPHERSON, H. 1980 The attenuation of water waves over a non-rigid bed. *J. Fluid Mech.* **97**, 721–742.

MEI, C. C., STIASSNIE, M. & YUE, D. K.-P. 2005 *Theory and Applications of Ocean Surface Waves.* World Scientific.

NG, C.-O. 2000 Water waves over a muddy bed: a two-layer Stokes' boundary layer model. *Coastal Engng.* **40**, 221–242.

OTT, E. & SUDAN, R. N. 1970 Damping of solitary waves. *Phys. Fluids* **13**, 1432.

PEREGRINE, D. H. 1972 Equations for water waves and the approximations behind them. In *Waves on Beaches and the Resulting Sediment Transport* (ed. R. E. Meyer), pp. 95–121. Academic

WEN, J. & LIU, P. L.-F. 1998 Effects of seafloor conditions on water wave damping, in *Free-Surface Flows with Viscosity* (ed. P. A. Tyvand). Computational Mechanics Publications.

YAMAMOTO, T., KONING, H. L., SELLMEIGHER, H. & HIJUM, E. V. 1978 On the response of poro-elastic bed to water waves. *J. Fluid Mech.* **87**, 193–206.